Electrochemically induced Ostwald Ripening in Au/TiO_2 Nanocomposite

Xiao Liu[1,2], Daniel G. Stroppa[3,4,†], Marc Heggen[3,4], Yury Ermolenko[5], Andreas Offenhäusser[1,2], and Yulia Mourzina[,1,2]*

[1] Peter Grünberg Institut-8, Forschungszentrum Jülich GmbH, 52425 Jülich, Germany

[2] Jülich Aachen Research Alliance (JARA)-Fundamentals of Future Information Technology, 52425 Jülich, Germany

[3] Peter Grünberg Institut-5 and [4] Ernst Ruska-Center, Forschungszentrum Jülich GmbH, 52425 Jülich, Germany

[5] Institute of Chemistry, St. Petersburg State University, 199034 St. Petersburg, Russia

[†] Present address: INL - International Iberian Nanotechnology Laboratory, 4715-330 Braga, Portugal

ABSTRACT: The report describes the Ostwald ripening process in a nanocomposite comprising gold nanoparticles and TiO_2 semiconductor under electrochemical conditions. The phenomenon is considered in relation to previous observations on the Ostwald ripening process in metallic nanostructures. Possible processes involved are discussed and a mechanism is proposed based on the size dependence of the electrochemical parameters of gold nanostructures.

Keywords: metal/semiconductor interface, nanoparticle growth, Ostwald ripening, size effect.

1 Introduction

The characteristic features of the electrochemical behavior of metallic nanoscopic objects, which are thermodynamically related to their morphology, surface atomic arrangement, and coordination, are of special interest for electrochemical synthesis and applications in the field of sensors as well as electro- and photocatalysis.[1-12]

One of the essential features of nanoscale metallic materials is the Ostwald ripening process,[13] which originally described the growth of larger objects (with a lower free energy) of one phase at the expense of smaller ones (with a higher free energy) in a two-phase system. Although not often documented in nanocomposite systems so far, Ostwald ripening may play an important role in the synthesis and application of nanocomposite materials incorporating metallic NPs, which change their functional, structural, optical, and electrochemical properties due to the size effect.[2, 9, 14-18]

A polydisperse colloidal system is not thermodynamically stable since the large interfacial area is a source of free energy, and therefore further stabilization may be achieved by the reduction of the interfacial area.[19] For smaller particles, the contribution of "curved surfaces" to the particle interfacial area increases, and the excess surface energy of smaller particles becomes more important in making a non-negligible contribution to the Gibbs free energy, resulting in a higher chemical potential.[20] Consequently, the equilibrium solute concentration at the surface of smaller particles in a polydisperse colloidal system is higher than for larger particles, and the driving force of Ostwald reforming is the dependence of the interfacial concentrations on the

curvature of the interface and, accordingly, the difference in solubility between polydisperse particles in accordance with the Ostwald-Freundlich equation[21]:

$c_S(r) = c_\infty \cdot exp\ (2\gamma V_m/RTr)$, where $c_S(r)$ *is* the solubility of a particle of size r, $c_\infty = c_S\ (r = \infty)$, γ is the interfacial tension, V_m is the molar volume of the precipitate, T is the absolute temperature, and R is the gas constant. The solubility differences establish concentration gradients between the concentrations of solutes at the particle surfaces in polydisperse colloidal systems which leads to transport of the solute, e.g., metal ions, from the smaller particles to the larger particles.[22] Thus, dissolution of smaller crystals or sol particles and the redeposition of the dissolved species on the surfaces of larger crystals or particles occurs, which reduces the overall free energy associated with the particle-matrix interfacial area. The rate of this aging process is determined by the size distribution of the precipitate, its growth kinetics, and the properties of the electrolyte and/or support or matrix.

Following the nucleation stage,[23] Ostwald ripening as an important crystal growth or coarsening mechanism was quantified by Lifshitz and Slyozov[24] and Wagner[25] in the LSW theory. The LSW theory was used to describe the coarsening of various colloids, for example, Au NPs, ZnO, CdS, InAs, and CdSe nanocrystals.[20, 22, 26,] The progress of Ostwald ripening theories has been reviewed in a number of published works.[20, 27-28]

In recent years, crystal growth and nanoparticles transformations cannot be explained or fitted by the Ostwald ripening model through the transport of monoatomic species between individual particles. Particle-mediated growth, assembly, and transformation mechanisms through the migration and coalescence of particles, such as oriented attachment and mesocrystal

formation, have been proposed as alternative mechanisms to explain "non-classical crystallization".[21, 29, 30]

Even so, Ostwald ripening remains an essential mechanism in the growth and transformation processes of particulate matter, such as colloidal metal growth and reforming,[17, 26] solution synthesis of quantum dots,[31] formation of solid dendrites, grain refining of microstructures, and reducing microsegregation of alloying elements, and it is now widely employed in materials processing and catalysis.[26, 28, 32] In recent years, multiple rounds of Ostwald ripening have become a matter-relocation approach to create a new kind of functional nanostructured materials with interior cavities - "hollow structures".[33] In contrast, by suppressing Ostwald ripening of cluster catalysts via atomic control of particle size (using particles with identical size Pt_{68} and the elimination of size selection), a Pt catalyst with high sintering resistance was achieved.[34] In addition, the much higher stability of magic-size nanocrystals (MSC) compared to nanocrystals of any intermediate size in a sample with a wide size distribution makes MSC stable with respect to Ostwald ripening.[35]

Several studies have demonstrated the role of chemical and photochemical oxidative and reductive conditions in transformations of nanoparticles by the Ostwald ripening mechanism.[36-38] The studies reported on oxygen-induced sintering of Pt NPs in Al_2O_3 matrixes mediated by an Ostwald ripening process,[36] and the influence of reducing agents such as hydroquinone[37] and resorcinol on Ostwald ripening of silver nanoparticles dispersed within pores of nanosized zeolite Y.[38] These findings suggest that the gradient of electrochemical potentials and reductive/oxidative conditions as well as operating electrochemical cells and devices in cycling modes (e.g., electrolysis-fuel cell, charge-discharge, and regeneration)[39-42] may play an essential

role in transformations of nanocomposites and electrochemical interfaces, while their role in Ostwald reforming of nanostructures in electrochemical cells needs to be further elucidated.

This work reports a new process of electrochemically induced Ostwald ripening in a metal/semiconductor nanocomposite material, which could represent a general phenomenon occurring in materials and heterojunctions involving the use of metal nanoparticles under electrochemical conditions.

2 Experimental

2.1 Materials

$HAuCl_4 \cdot 3H_2O$, TiO_2 (P25), oleylamine (OA), toluene, ascorbic acid (AA), sulfuric acid, ethanol, acetone, and indium tin oxide (ITO) electrodes were purchased from Sigma-Aldrich Chemicals and used as received. Distilled water was used throughout and other chemicals were reagent grade.

2.2 Apparatus

Electrochemical experiments were performed in a three-electrode setup controlled by a potentiostat (AUTOLAB, The Netherlands). Three-electrode systems were composed of either ITO or thin-film gold or Si/SiO_2 working electrodes modified with gold nanostructures or a TiO_2/Au nanocomposite (diameter of the electrode in the electrochemical cell was 0.5 cm), a platinum coil counter electrode, and an Ag/AgCl reference electrode (3 M KCl, $E^f = 0.210$ V vs NHE). The values of potentials were recorded against an Ag/AgCl reference electrode. Scanning electron microscopy (SEM) of the nanostructures was carried out using a Zeiss Gemini 1550 device. Transmission electron microscopy (TEM) was performed using an FEI TECNAI F20

analytical microscope equipped with a Tridiem energy filter. UV-visible absorption spectra were obtained by a Perkin-Elmer Lambda 900 instrument.

2.3 Electrode preparation

ITO-coated glass electrodes (R_s = 8-12 Ω/sq) were diced 11x11 mm and cleaned by immersion in distilled water, acetone, ethanol, and distilled water for 5 minutes, followed by ultrasound for 10 seconds in every solution.

The thin-film gold electrodes were prepared on Si/SiO_2 (SiO_2 1 μm) substrates. A titanium adhesion layer (10 nm thick) and gold films of 300 nm were deposited on Si/SiO_2 substrates by sputter deposition and diced as 11x11 mm substrates. Thin-film gold electrodes were cleaned in acetone, propanol, water, and 1:2 v/v of H_2O_2:H_2SO_4, followed by electrochemical cleaning and water.

The Si/SiO_2 substrate was diced 11x11 mm and cleaned in acetone, propanol, water, followed by1:2 v/v of H_2O_2:H_2SO_4 and water.

Electrodes were blown dry with nitrogen or pressed air.

2.4 Synthesis of Au nanostructures and Au/TiO_2 nanocomposite

The Au nanostructures were synthesized following slight modifications to the procedure.[43] Oleic acid was replaced by OA, according to the report on the effect of OA and oleic acid on the aspect ratio of nanostructures.[18] The cleaned and dry ITO or thin-film gold electrodes or Si/SiO_2 substrates, all 11x11mm, were introduced into the reaction vessel. 35 mg $HAuCl_4 \cdot 3H_2O$ was mixed with 300 μL OA in 25 mL toluene added to the vessel and the mixture was refluxed at

about 110 °C (boiling temperature of toluene) until the color of the solution changed from a yellowish color to completely colorless. After the solution cooled to room temperature, 20 mg AA in 12 mL toluene was added to the mixture. Then, the reaction mixture was aged for three hours to three days in the presence of AA, resulting in the formation of Au nanowires (NWs) or NPs on the electrodes.

The Au/TiO_2 nanocomposite was prepared by slightly varying the method for Au nanostructure synthesis (Scheme 1). 25 mg TiO_2 was firstly dissolved in 25 mL toluene and kept in ultrasound for 8 min, then 35 mg $HAuCl_4 \cdot 3H_2O$ in 10 mL toluene was added and the mixture was stirred overnight. 300 μL OA was added to the mixture the next day. The following procedure was the same as the Au NPs synthesis described above. The mixture was aged for three days.

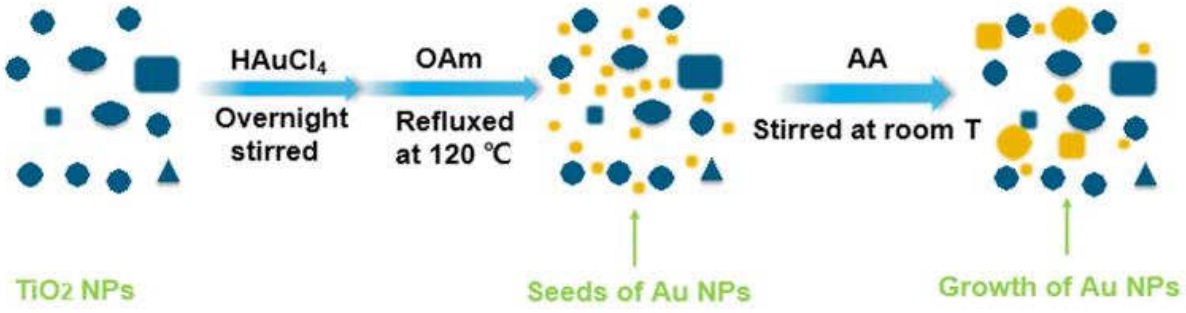

Scheme 1. Experimental process for the synthesis of Au/TiO_2 nanocomposite.

2.5 UV-visible absorption spectra of Au/TiO_2 nanocomposites

During the Au/TiO_2 nanocomposite synthesis procedure, the intermediate solutions for every step were characterized by UV-visible absorption spectroscopy. Two reference solutions containing 3.5 mL toluene and 30 μL OA were detected firstly as the background, then 0.5 mL one reference solution was replaced with 0.5 mL intermediate solution or final solution of the

Au/TiO_2 nanocomposite synthesis. The UV-visible absorption spectra of Au/TiO_2 nanocomposites were recorded during different steps of synthesis procedure and are shown in figure 1 (A).

2.6 Treatment and electrochemical experiments with Au/TiO_2 nanocomposite modified electrodes

After extracting the ITO electrodes from the Au/TiO_2 nanocomposite solution, they were immersed in ethanol, distilled water, and acetone for 2 minutes, respectively, to remove OA and AA. Then, they were dried at 100 °C for 2 hours. Cyclic voltammograms (CVs) of the nanocomposites on ITO were recorded in 0.1 M H_2SO_4 in the potential range between 0 V and 1.5 V with a scan rate of 50 mV s^{-1}.

2.7 Electrochemical experiments with Au nanostructure-modified electrodes in H_2SO_4

CVs of thin-film gold electrodes or Si/SiO_2 substrates modified with gold nanostructures as described above were recorded in 0.1 M H_2SO_4 in the potential range between 0 V and 1.5 V with a scan rate of 50 mV s^{-1}. After extracting the samples from the nanostructure solutions, the modified electrodes were cleaned by immersing them in ethanol, distilled water, and acetone for 2 minutes respectively to remove OA and AA. They were then dried at room temperature. Au NWs on Si/SiO_2 substrates were contacted using a contact paste outside the electrochemical cell.

2.8 SEM characterization of Au/TiO_2 nanocomposites and Au nanostructures

The surface morphologies of Au/TiO_2 nanocomposites and Au nanostructures were characterized by SEM before and after electrochemical experiments.

3 Results and Discussion

3.1 Electrochemically induced reforming in a nanocomposite comprising gold nanoparticles and TiO_2 semiconductor

A new TiO_2/Au nanocomposite material was prepared by modification of synthesis.[18, 43] Plasmonic metal nanostructures/TiO_2 nanocomposites prepared by other methods were recently discussed with respect to the conversion of solar to chemical energy.[6, 44, 45] The formation mechanism of gold nanostructures is based on the intrinsic property of Au (I) ions to form aurophilic interactions stabilized by OA, where Au (I) is subsequently reduced and sterically stabilized by OA molecules.[43, 46, 47] Before OA is added and the reaction with OA proceeds, the gold is adsorbed on the surface of TiO_2 (P25) NPs producing nucleation sites for the subsequent growth of gold nanostructures. The gold nanoparticles grow in the solution as well. After preparation, samples are washed with solvents and water to remove the stabilizing agent. The structural and spectral characterization of the nanocomposite material is presented in figures 1, 2 (A, B) and S1. The NPs were polycrystalline with a diameter of 11.5 nm (Figure S2).

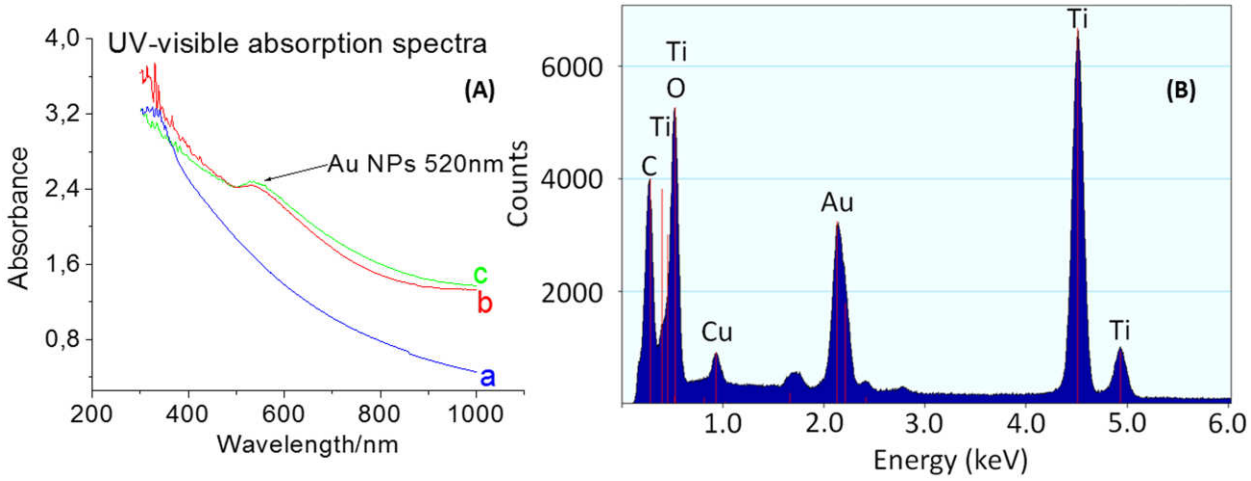

Figure 1. (A) UV-visible absorption spectra of Au/TiO_2 nanocomposites during different steps of synthesis procedure: (a) after $HAuCl_4 \cdot 3H_2O$, TiO_2 and OA were mixed in toluene, refluxed and cooled; (b) after AA was added and the mixture was aged for 2 days; (c) after AA was added and the mixture was aged for 15 days. (B) EDX spectra of Au/TiO_2 nanocomposite.

Electrochemically induced reforming or Ostwald ripening of gold NPs in the nanoporous semiconductor matrix took place during electrochemical characterization in the dark (Faraday cage) (Figures 2, S1 and S3). The structural changes were monitored by means of SEM. As follows from figure 2, the size of the gold NPs incorporated into the semiconductor matrix increased significantly up to 200 nm in diameter during electrochemical cycling between 0 V and 1.5 V (Ag/AgCl, 3 M KCl), preserving the NP form. The size dispersion of the NPs increased as well. However, reforming was not observed in our electrochemical studies on gold NPs ($d \approx 12$ nm) on flat surfaces of ITO (Figure S4), or on polycrystalline thin-film gold electrodes (Figure S5), or in the case of gold ultrathin NWs ($d \approx 2$ nm) on Si/SiO_2 (Figure S6) without a semiconductor nanoporous matrix.

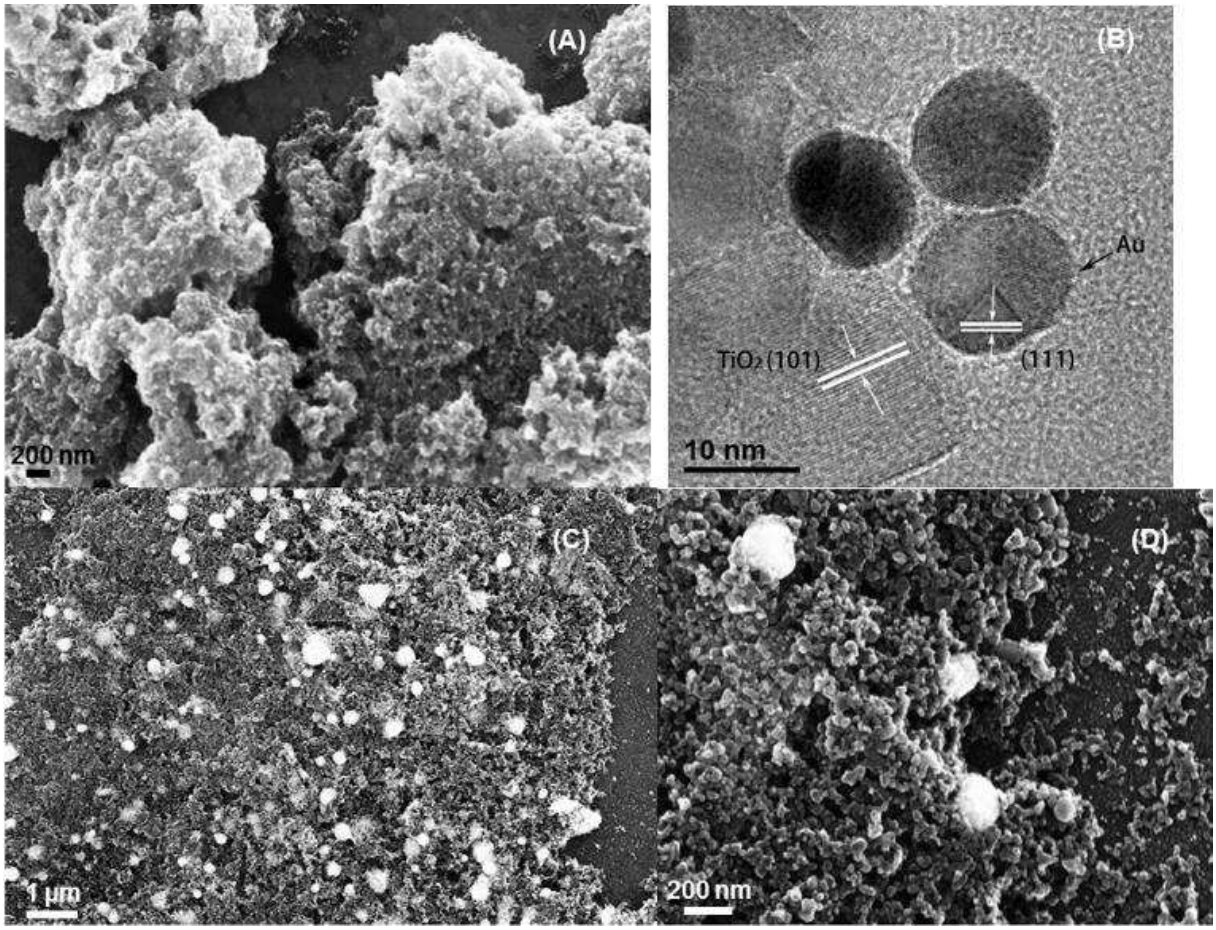

Figure 2. SEM images of Au/TiO_2 nanocomposites (A) before and (C, D) after 14 scans of electrochemical cycling in 0.1 M sulfuric acid; scan range 0 V to 1.5 V (Ag/AgCl, 3 M KCl); scan rate 0.05 Vs^{-1}. (B) HRTEM image of Au/TiO_2 nanocomposites before electrochemical cycling. Bright small spheres in the image (A) correspond to gold nanoparticles with a diameter of about 12 nm in TiO_2 matrix. Additional larger scale SEM and TEM images are provided in figure S1.

3.2 Size-dependence of redox properties of metallic nanostructures

First, the electrochemical features of gold nanostructures will be discussed, as this helps to explain the observed process of nanocomposite reformation. Theoretical and experimental

studies reported a negative (cathodic) size-dependent shift of the redox potential of metal/metal ion electrodes in metal colloids in relation to that of the bulk metal of up to several hundred millivolts, figure 3, (e.g., $E^0_{Ag+/Ag0(aq.)}$ of -1.8 V).[2, 48] This shift is an electrochemical manifestation of the shift of the work function, Φ^m, of metallic nanostructures. Usually, the results are discussed in terms of either the work function or Fermi energy, E_F^m, where

$$\Phi^m = -\tilde{\mu}_e^m - e_0\psi^m = -(\tilde{\mu}_e^m)_{q=0} = -(E_F^m)_{q=0} \quad (1),$$

identifying the work function of an electron in metal when it is charge-free (zero excess electrostatic charge) with the Fermi energy of the charge-free metal[40,49] where $\tilde{\mu}_e^m = \mu_e^m - e_0\varphi^m = \mu_e^m - e_0(\psi^m + \chi^m)$ (in eV), $\tilde{\mu}_e^m$ and μ_e^m are the electrochemical and chemical potential of an electron in metal, φ^m and ψ^m are the inner and outer (due to excess electrostatic charge on the phase) potentials, respectively, and χ^m is the surface potential of the metal in the charge-free state in contact with a vacuum[49,50], and e_0 is the elementary charge. In general case, the charge of a metal as a bulk or colloidal[51, 52] electrode is not zero ($\psi^m \neq 0$) in electrochemical studies; the charge is supplied to the metals, for example as an external applied potential.[53, 54] The presence of the charge causes the whole energy band to shift:

$$E_F^m = \tilde{\mu}_e^m = -(\Phi^m + e_0\psi^m) \quad (2).$$

Therefore, it makes sense to use the electrochemical potential scale in electrochemical systems to easily reference the electrochemical potentials and energy levels of electrons in redox systems [SI-Note (1)] on electrochemical, absolute potential (V), or physical (eV) scales.[53] This makes it easier to compare electrochemical potentials or the energy of electrons in various electrochemical processes [SI-Note (2)] (condition for electrochemical equilibrium between two solid or liquid

phases $\tilde{\mu}_e^{(1)} = \tilde{\mu}_e^{(2)}$)[49] and redox couples, where E_F^m can be fixed, for example, by an electrode attached to the material under study.

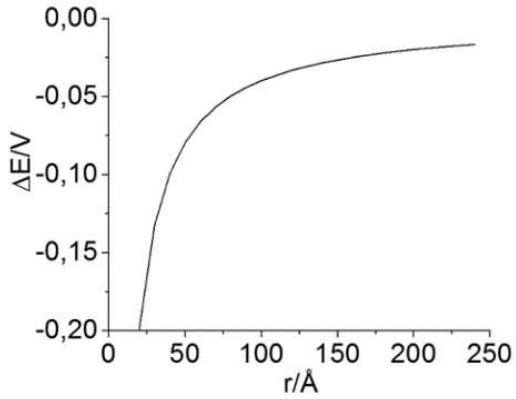

Figure 3. ΔE-radius calculated for Au NPs.

Qualitatively, using a galvanic cell to compare the potential scale of a metal in different modifications,[2, 55] Plieth showed that the whole electrochemical potential scale of the dispersed matter is shifted by the same value, $-\Delta\varepsilon_D$, as the reversible redox potential (Figure 4). $\Delta\varepsilon_D$ can be calculated as a voltage of an electrochemical cell with an electrode transfer reaction of one mole bulk metal into the dispersed form using an analogue of the Kelvin equation [2, 55, SI-Note (3)]:

$$\Delta\varepsilon_D = -\Delta G_D/zF = -2\gamma\upsilon_M/zFr \qquad (3),$$

where ΔG_D is the free energy of dispersion associated with the change in surface area, and γ, υ_M, z and r are the surface energy, the molar volume, the lowest valence state, and the radius of NPs, respectively. At 25 °C, γ_{Au} = 1880 erg cm^{-2}, $\upsilon_{M\ Au}$ = 10.21 cm^3 mol^{-1}, z_{Au} = 1. Thus, the electrochemical scale of the dispersed colloidal metal (d≤ appr.25 nm), including reversible redox metal/metal ion potential, oxidation and reduction potentials, and the potentials of adsorption and desorption[54] should shift by the same voltage $\Delta\varepsilon_D$ under the above-mentioned

assumptions.[2, 55, SI-Note (3)] This is schematically shown in figure 4, which is in a first approximation given by surface binding becoming vacant effecting essentially electronic properties.

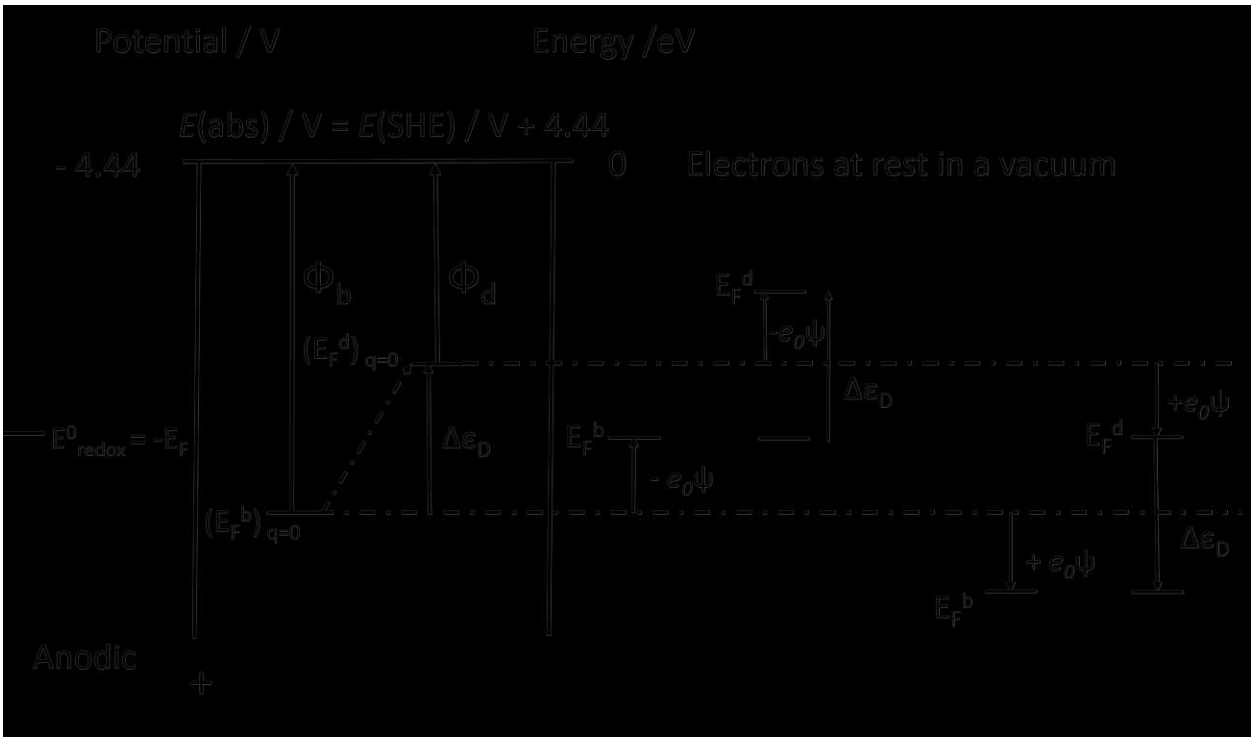

Figure 4. Comparison of electrochemical and energy scales for bulk and dispersed matter.

Thus, the shift of the oxidation potential in the cathodic direction indicates easier oxidation of metal particles.[2, 54, 56] The shift of the reduction potential in the cathodic direction is a manifestation of larger overpotential or additional energy, which is supplied to reduce the metal ions into the dispersed state in comparison to reduction into the bulk state. If Au^+ is reduced into the nanoparticulate form or if it is reduced on the gold NP surface, which has a higher Fermi level than a bulk electrode material (at the same charge, "$E_F^{Au\ NP}$" > "E_F^{Au}"), additional electrochemical energy (negative shift of the potential corresponds to higher energy on the energy scale) would be consumed as dispersion energy, ΔG_D, of the produced or growing Au

NPs (Au^0_{NP}) and the creation of electrified interfaces. Hence, metal ions are more difficult to reduce (they are reduced at more negative potential) into the nanoparticulate form with diameters of up to about 25 nm. The existence of a positive interfacial energy increases the energy required to form small particles with high curvature (higher Gibbs-Thomson potential). As will be shown later, these observations on the electrochemical behavior of nanostructures are important for explaining nanocomposite reformation.

Although there are few electrochemical studies on redox behavior as a function of the size and shape of nanostructures, a negative shift of the oxidation potentials (easier oxidation) of the citrate-stabilized silver NPs[56-58] and spontaneous Ostwald ripening of silver NPs[17] observed experimentally are explained using eq. (3). And a shift of the reduction potential in the cathodic direction due to the size of the NPs has been confirmed in a few publications[57, 59-60] (See Supporting Information). In this sense, gold nanostructures of different sizes behave like colloidal electrodes with different size-dependent reversible metal/metal ion potentials and E_F^m (Figure 4).

3.3 Mechanisms of NPs reforming

Based on the above data, we propose the following mechanism of electrochemically induced NPs reforming in the nanocomposite. The metal particles in the nanocomposite were not uniform in their energy and meal/metal ion potential. Some particles were more stabilized due to interaction with the TiO_2 matrix, which reduced their free surface energy (e.g., greater stability against electrochemical oxidation was observed for Ag clusters on graphite than for bulk metal[61]) and some particles had slightly larger diameters within the statistical distribution. These particles were therefore more stable to oxidation. In the course of the potential scan 0 → 1.5 V, the

particles with a higher surface energy (i.e., with a larger shift of the redox potential, $|\Delta\varepsilon|$, in the cathodic direction; probably those grown in the solution phase during synthesis and not stabilized by the interaction with TiO_2 matrix) were oxidized first, producing Au (I). The particles with a lower energy stabilized by TiO_2 and larger particles acted as reprecipitation (reduction) centers for the produced Au (I). On these stabilized or larger particles, reduction of Au (I) to Au (0) preferably took place. Thus, the Au (I) produced in the anodic scan from the particles not stabilized by interaction with a TiO_2 matrix and the smaller ones were reduced on the particles stabilized by interaction with TiO_2 matrix during the cathodic scan, due to the difference in the electrochemical potentials. The increased size dispersion mentioned above (Figure 2) may be explained by "interparticle diffusion coupling" (IDC).[62] As the process proceeded, the size of the dissolving particles was reduced and they became more and more thermodynamically unstable. Thus, the potential scan differentiated Au NPs with a different surface energy of NPs in the nanocomposite as oxidized (larger $|\Delta\varepsilon|$ values) and more stable (smaller $|\Delta\varepsilon|$ values) NPs, identifying the latter as the centers of electrochemical reprecipitation.

This was confirmed by the fact that reforming cannot take place without an applied potential (Figures 5, 6, and S8-S10). As will be seen from the discussion below, external applied voltage, which is necessary for the Au NPs to generate Au (I), is specific to this metal, but was not necessary, for example, to reform Ag NPs where the presence of Ag^+ was also necessary, as follows from the mechanisms proposed.[63, 17] However, Ag is a less inert metal than gold and it is more easily oxidized and solved in ambient conditions or Ag^+ was produced by other means without an external electric field.

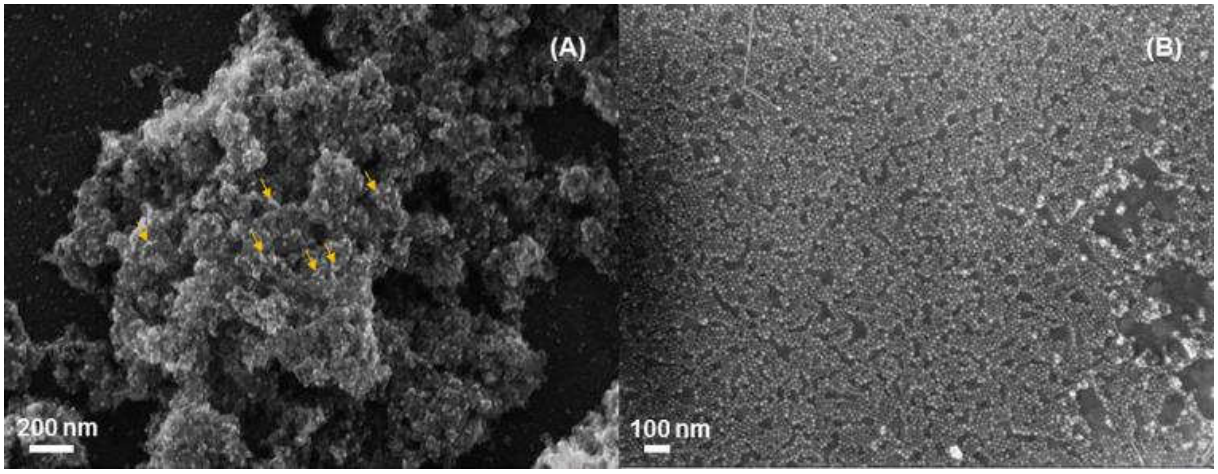

Figure 5. SEM images of (A) the Au/TiO_2 nanocomposites on ITO after immersion in the growth solution for 9 weeks (arrows mark the aggregated Au NPs) and (B) Au NPs grown on a gold substrate by the same method after immersion for 2 weeks. Bright small spheres in the image (A) correspond to gold nanoparticles with a diameter of about 12 nm in TiO_2 matrix. Larger scale image of figure 5 (A) is provided in figure S8.

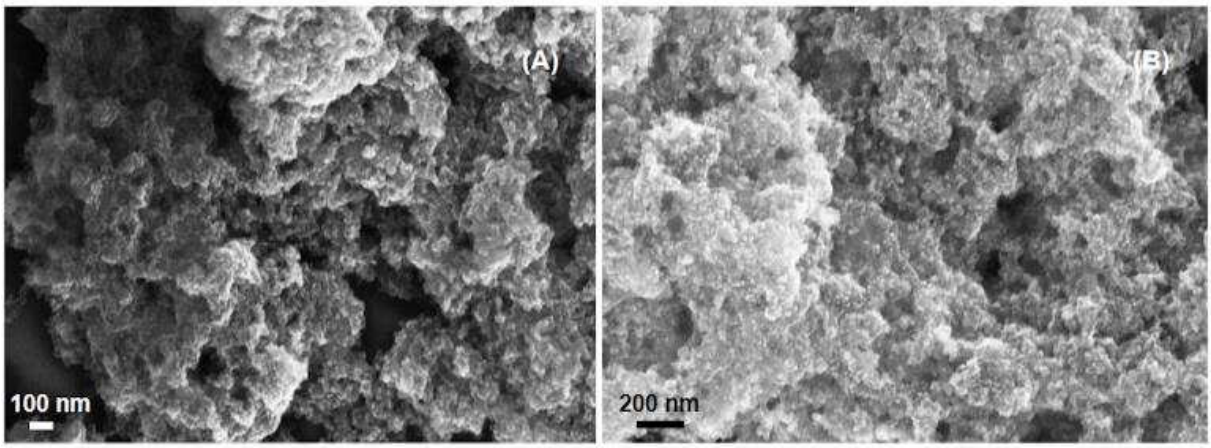

Figure 6. SEM images of Au/TiO_2 nanocomposites in 0.1 M sulfuric acid without applied potential (A) under light and (B) without light for 4 days. Bright small spheres on the images correspond to gold nanoparticles with a diameter of about 12 nm in TiO_2 matrix. Larger scale images of figure 6 (A) and (B) are provided in figure S9 and figure S10, respectively.

No structural changes in nanostructures that would be similar to Ostwald ripening were observed in gold nanostructures on ITO (Figure S4), thin-film gold electrodes (Figure S5), or Si/SiO_2 (Figure S6) during electrochemical cycling. Figure S5 shows that the size and form of the gold NPs remaining on the thin-film gold electrode surface after electrochemical cycling does not change significantly. We believe that this is due to the incorporation of the reduced gold atoms (which were oxidized on the surface of NPs during the anodic scan) into the thin-film gold substrate[40] during the cathodic scan. Furthermore, the reforming process was not observed for gold NPs grown on ITO or gold NWs on Si/SiO_2 substrates (Figures S4 and S6), but dissolution of some nanostructures occurred.

Reforming of gold NPs in nanocomposites only occurs upon application of an external potential. Figures 5 and S8 show SEM images of the nanocomposite on an ITO substrate after immersion in the growth solution for 9 weeks, and, for comparison, micrographs of gold NPs grown by the same method (without a semiconductor) on a gold substrate after immersion for 2 weeks (without application of an eternal potential). Only slight changes are visible in the gold nanostructures after 9 weeks in the nanoporous matrix of the semiconductor (some gold nanostructures were transformed to nanorods which were marked by arrows). These changes can be explained by slow long-term aggregation of NPs, similar to those reported in the literature. Moreover, reforming does not take place under acidic conditions, e.g. 0.1 M H_2SO_4, without application of an external potential in the dark or in light (Figures 6, S9 and S10).

It is important to discuss the results of studies on electrochemical growth and reforming and the application of external fields to structurally control the metal NPs in order to understand the factors and mechanisms that contribute to particle size and structural dispersions in electrochemical systems.

Spontaneous reforming of silver NPs on conductive surfaces in pure water[17] and silver NPs reforming on non-conductive substrates under photoirradiation accelerated by the electric field[63] have been reported in the literature. Interestingly, the presence of silver ions (Ag^+) in the solutions ("metal dissolution") was necessary in both cases for reformation. The reformation processes essentially proceeded via dissolution and redeposition of silver ions on neighboring particles. Possible sources of silver ions are the dissolution of either the Ag_2O layer covering the Ag NPs,[17, 63] which can be slightly solved in water and is readily attacked by acids, or silver metal dissolution in acidic conditions. Accordingly, the reformation process described by Redmond et al.[17] was accelerated in acidic media or by adding silver nitrate as an additional source of silver ions. Silver ions therefore initiate the reaction. In the mechanism proposed by Redmond et al.,[17] the larger and smaller particles behave as different metals with different standard potentials (size dependence of electrochemical properties as discussed in section 3.2). They form galvanic cells with a concentration gradient of silver ions when connected by a conductive substrate due to the greater work function of larger particles and the redox potential difference. In the work of Murakoshi et al.,[63] illumination is suggested as a method of reducing silver ions on a non-conductive substrate where there are no electron conduction pathways (electron transfer) between the particles.[64] Electric fields may also accelerate the dissolution of silver due to water hydrolysis and local changes in the pH, thus providing a source of Ag^+ for particle growth.

In the case of the inert and less reactive gold,[65] the Ostwald ripening process was not observed under acidic conditions in the dark or in light (Figure 6). This means that Au (I) is also necessary for the process to proceed, as it requires the application of potential. This passive feature of our process (potential-driven process) resembles a light-driven reforming of Ag

nanospheres to nanoprisms of larger sizes.[12] In both cases, the energy supplied to the system is necessary to initiate and drive the reforming process, although the exact mechanism of the latter transformation might require further clarification.

It was demonstrated that morphology, structural defects, and facet surface energy strongly effect the electrochemical oxidation potentials of Ag NPs, and also significantly influence the size and shape evolution of Ag NPs in Ostwald ripening processes.[66] The authors proposed that the classical Ostwald ripening theory should be modified taking into account morphology and structural defects, as this would enable it to predict the evolution of the size and shape of metal NPs in solutions more accurately. We believe that differences in the lattice energy and surface potentials χ (due to surface dipoles) of nanometals of different modifications should also be taken into account.[55] The dependence of surface stability and the dynamics of surface structures on potential have already been studied for the two-dimensional Ostwald ripening of metal surfaces, on which large islands of one layer height grow at the expense of smaller ones.[67] Two atomic processes were found to be rate-determining in this reformation: the detachment from a kink site and atomic diffusion on flat surfaces between the islands. It was shown that atom surface mobility increases when the potential is scanned towards a higher positive potential and can be enhanced by adsorbates, which reduce the activation energy for transport. The influence of the electric field was explained by interaction of an electric field in the double layer with local surface dipole moments of adatoms and steps on surfaces. Similar effects should probably be included in studies of morphology-dependent[66] Ostwald ripening of metal colloids.

Recently, dendritic assembly of gold NPs was observed under reductive polarization (cathodic potentials) during fuel-formation electrocatalysis.[1] The mechanisms proposed were diffusion, collision, and coalescence of the entire particles, reducing catalyst dispersion.

Although the mechanism, conditions, and structural changes observed were different from those reported in the present report, it was also shown here that 1) an external source of energy like temperature or electrochemical energy may force transformation of the noble metal catalyst, and 2) studies on the morphological changes of nanocatalysts during electrochemical catalysis are essential to improve our understanding of the nanocatalyst behavior under electrochemical conditions.

A nanoporous matrix of TiO_2 plays an essential role in the electrochemically induced ripening of Au NPs, since it was not observed on flat surfaces. We assume that the large three-dimensional contact area of the interface between Au NPs and the nanoporous TiO_2 matrix provides stronger stabilization for the Au NPs, which remain attached to the TiO_2 surface while growing during electrochemical cycling. In contrast, a smaller contact area and probable lower adhesion between the Au NPs and the planar surfaces lead to the detachment of Au NPs, as we observed, for example, on ITO substrates and planar gold in Figures S4 and S5 or the incorporation of the reduced gold atoms into the thin gold film in the case of Au NPs on planar gold thin film substrates, Figure S5.[40]

There is growing interest in the quantitative investigation of factors which may influence the properties of metallic NPs on various supporting substrates and contribute to the stability and reforming properties of the Au NPs-support nanocomposites. We assume that one of the key aspects in answering this question is a metallic NPs-matrix interface and the adsorption (adhesive) energy of Au NPs on various solid supports.[68, 69] Further factors include the charge distribution and electronic properties of metallic NPs as a result of interaction with a support,[4, 70, 71] particle size and morphology, chemical reactivity, and oxygen adsorption on the interfaces,[72] which are also strongly related to the catalytic activity and stability of metallic NPs.[69] However,

although there are a number of studies on the properties of interfaces between metallic clusters or NPs and oxide supporting matrixes and their influence on the stabilization and reactivity of metallic NPs,[4, 70-75] a fundamental issue remains elusive, namely how support oxides affect the stability and reactivity of metallic NPs. Hence, the role of a supporting substrate as well as details of the Au NPs-support interface need to be further elucidated. We assume that similar reforming may be observed for other semiconductor or even insulator particles matrixes, such as SiO_2, Al_2O_3, CeO_2, TiO_2, and MgO.[38, 76] Our study will probably be employed in future investigations of the effect of the matrix on the stability and reactivity of metallic nanoparticles.

4 Conclusion

The new process of electrochemical Ostwald ripening outlined in this report has important consequences. Nanocomposites similar to those used here are expected to be widely used in solar energy conversion and catalysis,[6, 44, 45] both of which are essentially electrochemically governed processes in solutions. So far, the process we refer to as electrochemically induced Ostwald ripening has not been reported, but it could have direct implications for both catalytic and light-adsorbing properties of the transformed nanocomposite due to the size effect. This process may help to explain the behavior of semiconductor/metal nanocomposite materials and heterojunctions under electrochemical conditions. Furthermore, we anticipate that the same transformations could be observed for other material combinations.

AUTHOR INFORMATION

Corresponding Author

*Tel.: +49(0)2461612364 (Y.M.). E-mail: y.mourzina@fz-juelich.de.

Notes

The authors declare no competing financial interest.

ACKNOWLEDGMENT

Xiao Liu would like to thank the China Scholarship Council (File No. 201206890019) for financial support. Financial support from St. Petersburg State University Grant SPbGU № 12.38.218.2015 and RFBR №14-03-01079 is gratefully acknowledged.

ASSOCIATED CONTENT

Supporting Information Available.

Further details of TEM and SEM images, histogram of NP size distribution and cyclic voltamogramms. This material is available free of charge via the Internet at http://pubs.acs.org

REFERENCES

(1) Manthiram, K.; Surendranath, Y.; Alivisatos, A. P. Dendritic Assembly of Gold Nanoparticles during Fuel-Forming Electrocatalysis. *J. Am. Chem. Soc.* **2014**, *136*, 7237-7240.

(2) Plieth, W. J. Electrochemical Properties of Small Clusters of Metal Atoms and Their Role in the Surface Enhanced Raman Scattering. *J. Phys. Chem.* **1982**, *86*, 3166-3170.

(3) Henglein, A.; Lilie, J. Storage of Electrons in Aqueous Solution: the Rates of Chemical Charging and Discharging the Colloidal Silver Microelectrode. *J. Am. Chem. Soc.* **1981**, *103*, 1059-1066.

(4) Wood, A.; Giersig, M.; Mulvaney, P. Fermi Level Equilibration in Quantum Dot−Metal Nanojunctions. *J. Phys. Chem. B* **2001**, *105*, 8810-8815.

(5) Penner, R. M. Chemical Sensing with Nanowires. *Annu. Rev. Anal. Chem.* **2012**, *5*, 461-485.

(6) Linic, S.; Christopher, P.; Ingram, D. B. Plasmonic-Metal Nanostructures for Efficient Conversion of Solar to Chemical Energy. *Nature Mater.* **2011**, *10*, 911-921.

(7) Engelbrekt, C.; Jensen, P. S.; Sørensen, K. H.; Ulstrup, J.; Zhang, J. Complexity of Gold Nanoparticle Formation Disclosed by Dynamics Study. *J. Phys. Chem.* C **2013**, *117*, 11818-11828.

(8) Zhou, Z.-Y.; Tian, N.; Li, J.-T.; Broadwell, I.; Sun, S.-G. Nanomaterials of High Surface Energy with Exceptional Properties in Catalysis and Energy Storage. *Chem. Soc. Rev.* **2011**, *40*, 4167-4185.

(9) Li, Y.; Cox, J. T.; Zhang, B. Electrochemical Responses and Electrocatalysis at Single Au Nanoparticles. *J. Am. Chem. Soc.* **2010**, *132*, 3047-3054.

(10) Mulvaney, P.; Linnert, T.; Henglein, A. Surface Chemistry of Colloidal Silver in Aqueous Solution: Observations on Chemisorption and Reactivity. *J. Phys. Chem.* **1991**, *95*, 7843-7846.

(11) Proch, S.; Wirth, M.; White, H. S.; Anderson, S. L. Strong Effects of Cluster Size and Air Exposure on Oxygen Reduction and Carbon Oxidation Electrocatalysis by Size-Selected Ptn ($n \leq 11$) on Glassy Carbon Electrodes. *J. Am. Chem. Soc.* **2013**, *135*, 3073-3086.

(12) Jin, R.; Cao, Y.; Mirkin, C. A.; Kelly, K. L.; Schatz, G. C.; Zheng, J. G. Photoinduced Conversion of Silver Nanospheres to Nanoprisms. *Science* **2001**, *294*, 1901-1903.

(13) Ostwald, W. Studien ueber die Bildung und Umwandlung fester Koerper. *Zeitschrift f. physik. Chemie XXII*, 1897, 289-330.

(14) Jain, P. K.; Huang, X.; El-Sayed, I. H.; El-Sayed, M. A. Noble Metals on the Nanoscale: Optical and Photothermal Properties and Some Applications in Imaging, Sensing, Biology, and Medicine. *Acc. Chem. Res.* **2008**, *41*, 1578-1586.

(15) Murphy, C. J.; Sau, T. K.; Gole, A. M.; Orendorff, C. J.; Gao, J.; Gou, L.; Hunyadi, S. E.; Li, T. Anisotropic Metal Nanoparticles: Synthesis, Assembly, and Optical Applications. *J. Phys. Chem. B* **2005**, *109*, 13857-13870.

(16) Alivisatos, A. P. Nanocrystals: Building Blocks for Modern Materials Design. *Endeavour* **1997**, *21*, 56-60.

(17) Redmond, P. L.; Hallock, A. J.; Brus, L. E. Electrochemical Ostwald Ripening of Colloidal Ag Particles on Conductive Substrates. *Nano Lett.* **2004**, *5*, 131-135.

(18) Wang, C.; Hu, Y.; Lieber, C. M.; Sun, S. Ultrathin Au Nanowires and Their Transport Properties. *J. Am. Chem. Soc.* **2008**, *130*, 8902-8903.

(19) Kahlweit, M. Ostwald Ripening of Precipitates. *Adv. Colloid Interface Sci*. **1975**, *5*, 1-35.

(20) Viswanatha, R.; Sarma, D. D. *Growth of Nanocrystals in Solution. In Nanomaterials Chemistry*. Wiley-VCH Verlag GmbH & Co. KGaA, Weinheim, 2007, pp 139-170.

(21) Dalmaschio, C. J.; Ribeiro, C.; Leite, E. R. Impact of the Colloidal State on the Oriented Attachment Growth Mechanism. *Nanoscale* **2010**, *2*, 2336-2345.

(22) Hu, Z.; Oskam, G.; Searson, P. C. Influence of Solvent on the Growth of ZnO Nanoparticles. *J. Colloid Interface Sci*. **2003**, *263*, 454-460.

(23) LaMer, V. K.; Dinegar, R. H. Theory, Production and Mechanism of Formation of Monodispersed Hydrosols. *J. Am. Chem. Soc.* **1950**, *72*, 4847-4854.

(24) Lifshitz, I. M.; Slyozov, V. V. The Kinetics of Precipitation from Supersaturated Solid Solutions. *J. Phys. Chem. Solids* **1961**, *19*, 35-50.

(25) Wagner, C. Theorie der Alterung von Niederschlägen durch Umlösen (Ostwald-Reifung). Zeitschrift für Elektrochemie, *Ber. Bunsenges. Phys. Chem.* **1961**, *65*, 581-591.

(26) Thanh, N. T. K.; Maclean, N.; Mahiddine, S. Mechanisms of Nucleation and Growth of Nanoparticles in Solution. *Chem. Rev*. **2014**, *114*, 7610-7630.

(27) Baldan, A. Review Progress in Ostwald Ripening Theories and Their Applications to Nickel-base Superalloys Part I: Ostwald Ripening Theories. *J. Mater. Sci.* **2002**, *37*, 2171-2202.

(28) Ratke, L.; Voorhees, P. W. *Growth and Coarsening: Oswald Ripening in Material processing*, Springer: New York, 2002, pp 117-118.

(29) Niederberger, M.; Colfen, H. Oriented Attachment and Mesocrystals: Non-Classical Crystallization Mechanisms based on Nanoparticle Assembly. *Phys. Chem. Chem. Phys*. **2006**, *8*, 3271-3287.

(30) Penn, R. L.; Banfield, J. F. Imperfect Oriented Attachment: Dislocation Generation in Defect-Free Nanocrystals. *Science* **1998**, *281*, 969-971.

(31) Klimov, V. I. *Nanocrystal Quantum Dots, second edition*, CRC Press: Boca Raton, USA, 2010.

(32) Burlakov, V. M.; Kantorovich, L. Ostwald Ripening of Binary Alloy Particles. *J. Chem. Phys*. **2011**, *134*, 024521.

(33) Yec, C. C.; Zeng, H. C. Synthesis of Complex Nanomaterials via Ostwald Ripening. *J. Mater. Chem. A* **2014**, *2*, 4843-4851.

(34) Wettergren, K.; Schweinberger, F. F.; Deiana, D.; Ridge, C. J.; Crampton, A. S.; Rötzer, M. D.; Hansen, T. W.; Zhdanov, V. P.; Heiz, U.; Langhammer, C. High Sintering Resistance of Size-Selected Platinum Cluster Catalysts by Suppressed Ostwald Ripening. *Nano Lett*. **2014**, *14*, 5803-5809.

(35) Kudera, S.; et al. Sequential Growth of Magic-Size CdSe Nanocrystals. *Adv. Mater.* **2007**, *19*, 548-552.

(36) Simonsen, S. B.; Chorkendorff, I.; Dahl, S.; Skoglundh, M.; Sehested, J.; Helveg, S. Direct Observations of Oxygen-induced Platinum Nanoparticle Ripening Studied by In Situ TEM. *J. Am. Chem. Soc.* **2010**, *132*, 7968-7975.

(37) Gentry, S. T.; Kendra, S. F.; Bezpalko, M. W. Ostwald Ripening in Metallic Nanoparticles: Stochastic Kinetics. *J. Phys. Chem. C* **2011**, *115*, 12736-12741.

(38) Severance, M.; Dutta, P. K. Evolution of Silver Nanoparticles within an Aqueous Dispersion of Nanosized Zeolite Y: Mechanism and Applications. *J. Phys. Chem. C* **2014**, *118*, 28580-28591.

(39) Graves, C.; Ebbesen, S. D.; Jensen, S. H.; Simonsen, S. B.; Mogensen, M. B. Eliminating Degradation in Solid Oxide Electrochemical Cells by Reversible Operation. *Nat. Mater.* **2015**, *14*, 239-244.

(40) Bagotsky, V. S. *Fundmentals of Electrochemistry, second edition*; Wiley-Interscience, New York, USA, 2005.

(41) Sathiya, M.; et al. Origin of Voltage Decay in High-Capacity Layered Oxide Electrodes. *Nat. Mater.* **2015**, *14*, 230-238.

(42) Kirshenbaum, K.; Bock, D. C.; Lee, C.-Y.; Zhong, Z.; Takeuchi, K. J.; Marschilok, A. C.; Takeuchi, E. S. In Situ Visualization of $Li/Ag_2VP_2O_8$ Batteries Revealing Rate-Dependent Discharge Mechanism. *Science* **2015**, *347*, 149-154.

(43) Halder, A.; Ravishankar, N. Ultrafine Single-Crystalline Gold Nanowire Arrays by Oriented Attachment. *Adv. Mater.* **2007**, *19*, 1854-1858.

(44) Kowalska, E.; Abe, R.; Ohtani, B. Visible Light-induced Photocatalytic Reaction of Gold-modified Titanium (iv) Oxide Particles: Action Spectrum Analysis. *Chem. Commun.* **2009**, 241-243.

(45) Gomes Silva, C.; Juárez, R.; Marino, T.; Molinari, R.; García, H. Influence of Excitation Wavelength (UV or Visible Light) on the Photocatalytic Activity of Titania Containing Gold Nanoparticles for the Generation of Hydrogen or Oxygen from Water. *J. Am. Chem. Soc.* **2010**, *133*, 595-602.

(46) Kisner, A.; Heggen, M.; Fernández, E.; Lenk, S.; Mayer, D.; Simon, U.; Offenhäusser, A.; Mourzina, Y. The Role of Oxidative Etching in the Synthesis of Ultrathin Single-Crystalline Au Nanowires. *Chem. Eur. J.* **2011**, *17*, 9503-9507.

(47) Lu, X.; Yavuz, M. S.; Tuan, H.-Y.; Korgel, B. A.; Xia, Y. Ultrathin Gold Nanowires Can Be Obtained by Reducing Polymeric Strands of Oleylamine−AuCl Complexes Formed via Aurophilic Interaction. *J. Am. Chem. Soc.* **2008**, *130*, 8900-8901.

(48) Henglein, A. The Reactivity of Silver Atoms in Aqueous Solutions (A γ-Radiolysis Study). *Ber. Bunsenges. Phys. Chem.* **1977**, *81*, 556-561.

(49) Bockris, J. O. M.; Khan, S. U. M. *Surface Electrochemistry: A Molecular Level Approach*; Plenum Press: New York, London, 1993.

(50) Bard, A. J.; Faulkner, L. R. *Electrochemical Methods: Fundamentals and Applications, 2nd Edition*; Wiley, New York, USA, 2001.

(51) Henglein, A.; Fojtik, A.; Welter, H. Reactions on Colloidal Semiconductor Particles. *Ber. Bunsenges. Phys. Chem.* **1987**, *91*, 441-446.

(52) Bard, A. J.; Fox, M. A. Artificial Photosynthesis: Solar Splitting of Water to Hydrogen and Oxygen. *Acc. Chem. Res.* **1995**, *28*, 141-145.

(53) Trasatti, S. The Absolute Electrode Potential: An Explanatory Note. *Pure Appl. Chem.* **1986**, *58*, 955-966.

(54) Henglein, A. Physicochemical Properties of Small Metal Particles in Solution: "Microelectrode" Reactions, Chemisorption, Composite metal Particles, and the Atom-to-Metal Transition. *J. Phys. Chem.* **1993**, *97*, 5457-5471.

(55) Plieth, W. J. Correlations between the Equilibrium Potential and the Potential of Zero Charge of Metals in Different Modifications. *J. Electroanal. Chem. Interfacial Electrochem.* **1986**, *204*, 343-349.

(56) Ivanova, O. S.; Zamborini, F. P. Size-Dependent Electrochemical Oxidation of Silver Nanoparticles. *J. Am. Chem. Soc.* **2009**, *132*, 70-72.

(57) Chaki, N. K.; Sharma, J.; Mandle, A. B.; Mulla, I. S.; Pasricha, R.; Vijayamohanan, K. Size Dependent Redox Behavior of Monolayer Protected Silver Nanoparticles (2-7 nm) in Aqueous Medium. *Phys. Chem. Chem. Phys.* **2004**, *6*, 1304-1309.

(58) Koposova, E.; Kisner, A.; Shumilova, G.; Ermolenko, Y.; Offenhäusser, A.; Mourzina, Y. Oleylamine-Stabilized Gold Nanostructures for Bioelectronic Assembly. Direct Electrochemistry of Cytochrome c. *J. Phys. Chem. C* **2013**, *117*, 13944-13951.

(59) Sheridan, E.; Hjelm, J.; Forster, R. J. Electrodeposition of Gold Nanoparticles on Fluorine-Doped Tin Oxide: Control of Particle Density and Size Distribution. *J. Electroanal. Chem.* **2007**, *608*, 1-7.

(60) Hezard, T.; Fajerwerg, K.; Evrard, D.; Collière, V.; Behra, P.; Gros, P. Gold Nanoparticles Electrodeposited on Glassy Carbon using Cyclic Voltammetry: Application to Hg (II) Trace Analysis. *J. Electroanal. Chem.* **2012**, *664*, 46-52.

(61) Ng, K. H.; Liu, H.; Penner, R. M. Subnanometer Silver Clusters Exhibiting Unexpected Electrochemical Metastability on Graphite. *Langmuir* **2000**, *16*, 4016-4023.

(62) Penner, R. M. Mesoscopic Metal Particles and Wires by Electrodeposition. *J. Phys. Chem. B* **2002**, *106*, 3339-3353.

(63) Murakoshi, K.; Tanaka, H.; Sawai, Y.; Nakato, Y. Photoinduced Structural Changes of Silver Nanoparticles on Glass Substrate in Solution under an Electric Field. *J. Phys. Chem. B* **2002**, *106*, 3041-3045.

(64) Peyser, L. A.; Vinson, A. E.; Bartko, A. P.; Dickson, R. M. Photoactivated Fluorescence from Individual Silver Nanoclusters. *Science* **2001**, *291*, 103-106.

(65) Hammer, B.; Norskov, J. K. Why Gold is the Noblest of All the Metals. *Nature* **1995**, *376*, 238-240.

(66) Kuo, C. L.; Hwang, K. C. Does Morphology of a Metal Nanoparticle Play a Role in Ostwald Ripening Processes? *Chem. Mater.* **2013**, *25*, 365-371.

(67) Mesgar, M.; Kaghazchi, P.; Jacob, T.; Pichardo-Pedrero, E.; Giesen, M.; Ibach, H.; Luque, N. B.; Schmickler, W. Chlorine-Enhanced Surface Mobility of Au(100). *ChemPhysChem* **2013**, *14*, 233-236.

(68) Farmer, J. A.; Campbell, C. T. Ceria Maintains Smaller Metal Catalyst Particles by Strong Metal-Support Bonding. *Science* **2010**, *329*, 933-936.

(69) Suib, S. L. *New and Future Developments in Catalysis: Catalysis by Nanoparticles,* Elsevier: Chennai, India, 2013.

(70) Yang, Z.; Wu, R.; Goodman, D. W. Structural and Electronic Properties of Au on TiO_2 (110). *Phys. Rev. B* **2000**, *61*, 14066-14071.

(71) Choi, H.; Chen, W. T.; Kamat, P. V. Know Thy Nano Neighbor. Plasmonic versus Electron Charging Effects of Metal Nanoparticles in Dye-Sensitized Solar Cells. *ACS Nano* **2012**, *6*, 4418-4427.

(72) Liu, Z.-P.; Gong, X.-Q.; Kohanoff, J.; Sanchez, C.; Hu, P. Catalytic Role of Metal Oxides in Gold-Based Catalysts: A First Principles Study of CO Oxidation on TiO_2 Supported Au. *Phys. Rev. Lett.* **2003**, *91*, 266102.

(73) Haruta, M. Catalysis of Gold Nanoparticles Deposited on Metal Oxides. *CATTECH* **2002**, *6*, 102-115.

(74) van Bokhoven, J. A.; Louis, C.; Miller, J. T.; Tromp, M.; Safonova, O. V.; Glatzel, P. Activation of Oxygen on Gold/Alumina Catalysts: In Situ High-Energy-Resolution Fluorescence and Time-Resolved X-ray Spectroscopy. *Angew. Chem. Int. Ed.* **2006**, *45*, 4651-4654.

(75) Bond, G. C.; Louis, C.; Thompson, D. T. *Catalysis by Gold*, Imperial College Press: London, UK, 2006.

(76) Simonsen, S. B.; Chorkendorff, I.; Dahl, S.; Skoglundh, M.; Sehested, J.; Helveg, S. Ostwald Ripening in a Pt/SiO_2 Model Catalyst Studied by in situ TEM. *J. Catal.* **2011**, *281*, 147-155.

Table of Contents – Graphic